29 January 1982, Volume 215, Number 4532 SCIENCE

Scattered Electrons in Microscopy and Microanalysis

F. P. Ottensmeyer

Summary. The use of scattered electrons alone for direct imaging of biological specimens makes it possible to obtain structural information at atomic and near-atomic spatial resolutions of 0.3 to 0.5 nanometer. While this is not as good as the resolution possible with x-ray crystallography, such an approach provides structural information rapidly on individual macromolecules that have not been, and possibly cannot be, crystallized. Analysis of the spectrum of energies of scattered electrons and imaging of the latter with characteristic energy bands within the spectrum produces a powerful new technique of atomic microanalysis. This technique, which has a spatial resolution of about 0.5 nanometer and a minimum detection sensitivity of about 50 atoms of phosphorus, is especially useful for light atom analysis and appears to have applications in molecular biology, cell biology, histology, pathology, botany, and many other fields.

Electron microscopy is the most directly interpretable route to the study of subcellular structure and organization. Light microscopy lacks the resolution to image details of cellular organelles such as mitochondria, or of particles such as ribosomes or viruses. Solution techniques for ensembles of molecules, such as nuclear magnetic resonance or circular dichroism, have spatial resolution within the macromolecule but require the disruption of subcellular organization that microscopic techniques attempt to preserve. X-ray crystallographic techniques, capable of structure determination with the highest resolution, require regular arrays of identical structural entities—crystals.

The modern electron microscope is capable of resolving distances as small as interatomic spacings at about 0.2 to 0.3 nanometer. Figure 1 is an electron micrograph of a small chemical compound containing, among others, six medium heavy atoms, four of iodine and two of palladium, which are very well resolved (*1*). This micrograph, a composite of four individual images superposed, was obtained by using only scattered electrons, a still unconventional technique in electron microscopy which nevertheless has made the achievement of atomic resolution possible in several laboratories (*2*). However, for several reasons this degree of resolution is virtually never achieved in images of biological specimens obtained by conventional techniques. Electrons interact relatively poorly with light atoms such as carbon, nitrogen, and oxygen, of which biological matter is composed. This lack of interaction results in a lack of contrast or visibility of details within the specimen, which must be overcome by the use of heavy atom contrast agents in the usual technique of imaging called bright field microscopy (Fig. 2a). It is the packing of the heavy atom clusters in a thin metal shell around the specimen, or the arrangement of heavy atom ions permeating the specimen, that provides the visibility and also the resolution in the image. For uranyl acetate, a typical contrast agent, the uranyl ion has a diameter of about 0.9 nm, suggesting, according to the Nyquist sampling theorem (*3*), a possible resolution of about 2 nm. This is the limit generally observed and accepted in images of typical biological specimens such as the uranyl acetate stained–bacterial virus shown in Fig. 3.

This limit, although an order of magnitude worse than the potential resolution of the electron microscope, nevertheless is still about 200-fold better than the resolution of a light microscope. Thus, bright field microscopy has been singularly instrumental in the visualization and identification of viruses (for instance, Fig. 3), and has led to a degree of understanding of the morphology and function of normal and diseased cells and tissues that would have been impossible without it. Texts and atlases of histology, for instance, abound with electron micrographs, which are indispensable teaching adjuncts (*4*).

At resolution levels below 2.0 nm, the validity of the detail of the images comes into question for two reasons. The fidelity with which the heavy metal can outline finer details of the biological structure becomes progressively worse. But, in addition, a purely electron-optical effect due to lens limitations causes a rapidly fluctuating reversal of contrast that depends on the size of the specimen detail and on the focus setting of the microscope. In principle, this effect is well understood and under the complete control of the microscopist. In practice, the result is a "horrible hologram" to the biologist (*5*) and a delight only for the physicists, who have undertaken the difficult task of unraveling it by computer or optical image processing—in, indeed, very few cases (*6*, *7*).

Yet many biological structures have details of interest smaller than 2.0 nm. At this level, the substructure of biological macromolecules comes into prominence: the major domains, the grooves or clefts of potential catalytic sites, the tertiary or even secondary structure folding of amino acid chains, and the location of specific sites on the molecules, accentuated at times by heavy atom tags. Until re-

The author is a professor in the Department of Medical Biophysics, University of Toronto, and research physicist at the Ontario Cancer Institute, Toronto, Ontario, Canada M4X 1K9.

0036-8075/82/0129-0461$01.00/0

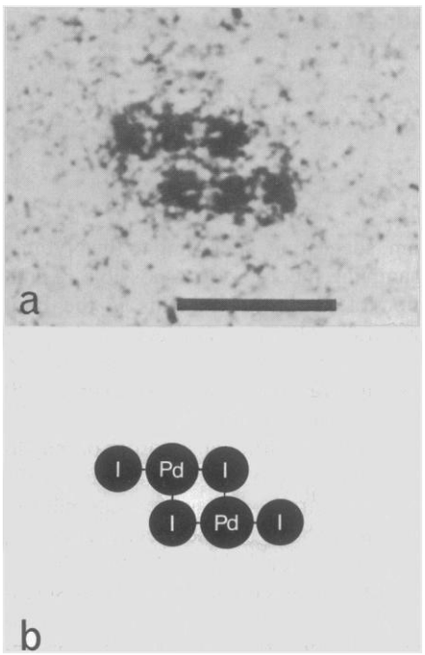

Fig. 1. Atom images of iodine and palladium covalently bound in a small chemical, *sym-trans*-di-μ-iododiiodobis(dimethylphenylarsine) dipalladium(II). (a) Superposition of four dark field micrographs with a 180° rotation to increase the signal-to-noise ratio. (b) Corresponding chemical structure of the heavier atoms in the molecule. Scale bar, 1.0 nm.

cently, only x-ray crystallography had the resolution to determine structures with such fine detail. Now, however, unconventional modes of electron microscopy, using only scattered electrons for imaging, have been developed to the point at which meaningful near-atomic detail at 0.3 to 0.5 nm is frequently observed in images of biological macromolecules.

Scattered electrons carry two bits of information from the specimen. The first, most commonly used bit is indicative of the location at which the scattering event took place. The second piece of information is in the proportion of electrons that have lost energy in the interaction with the specimen. This energy is imparted to the specimen by exciting molecules or atoms within it, and the spectrum of such energy losses is then characteristic of the atoms and molecules of which the specimen is composed. In standard electron microscopes only the spatial information can be used, but with accessory electron spectrometers, spatial and energy information can be separated and used individually or jointly to image, to analyze, or to map the chemical constituents within a specimen at very high spatial resolution and with great sensitivity.

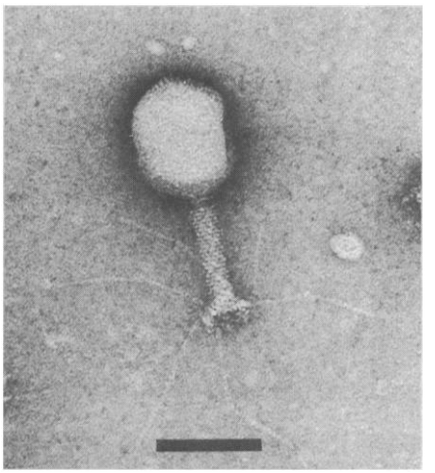

Fig. 3. Conventional bright field image of bacteriophage T4 stained with uranyl acetate. A wealth of morphological detail is seen, but the finest biologically interpretable details, the striations in the phage tail, have a spacing just over 2.0 nm. Scale bar, 100 nm.

Imaging with Scattered Electrons

All imaging in electron microscopy depends on the interaction of the illuminating electrons with the specimen. Conventionally, the main beam of uninteracted electrons is used to form a bright field or negative type of image by virtue of the removal of most of the electrons that are scattered by the specimen. The portion of scattered electrons that does contribute to the image produces phase-contrast effects by interacting with the main beam. These effects can accentuate image details of one size at the expense of details of another size at a given focus setting of the microscope, to help clarify or at times to confuse (*8*).

Since the scattered rather than the uninteracted electrons carry specimen information, electron microscopy with only scattered electrons appears to be a rational imaging approach, and it was considered shortly after the introduction of the electron microscope (*9*). However, successful imaging with scattered electrons alone is not easily achieved, requiring the simultaneous combination of several factors—specimen preparation, illumination, imaging conditions—each of which is substantially different from that in conventional bright field electron microscopy.

Imaging conditions with scattered electrons are obtained in at least six ways (*9, 10*), only three of which are shown in Fig. 2. In every case, the primary, undeflected electron beam is prevented from contributing to the image, producing a so-called dark field image. However, some precautions are vital to obtain good images. Since the region of the objective lens of the electron microscope is very sensitive to electrostatic and magnetic perturbations, methods that move the objective aperture off the optic axis or place a beam stop in the aperture in general deteriorate image resolution. Hollow cone illumination (Fig. 2b) and oblique illumination (Fig. 2c, a one-sided version of Fig. 2b) are more ideal and are still readily achieved in most modern transmission electron microscopes. The method in Fig. 2d, which at high resolution was pioneered by Crewe *et al.* (*11*), deserves special attention, since it represents the most efficient collection and use of scattered electrons. Here the unscattered beam passes through an annular aperture, while the electrons scattered by the specimen are captured on the aperture and processed electronically to produce

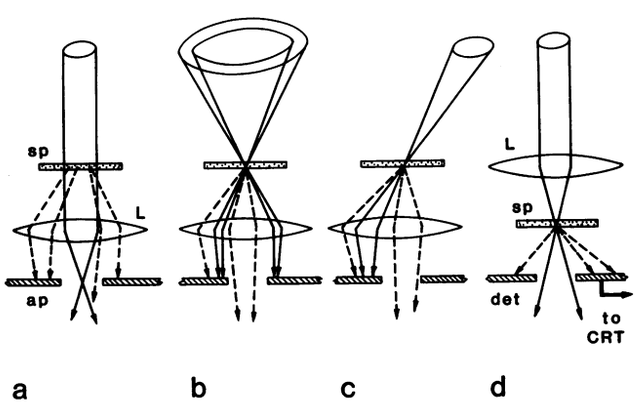

Fig. 2. Schematic of modes of using electrons to form images in electron microscopy. Heavy solid lines indicate the main beam of electrons, broken lines electrons scattered by the specimen (*sp*). (a) Bright field: the main beam is focused through the aperture (*ap*) by the objective lens (*L*) to form a negative image, since many of the scattered electrons are stopped by the aperture. (b) Dark field: the main beam in the form of the hollow cone is focused on the specimen, then stopped by the aperture rim. The image is formed by scattered electrons that pass through the aperture. (c) Dark field with a tilted beam, a one-sided version of (b). (d) Dark field with a finely focused scanning beam. The image is formed point by point on a cathode-ray tube (*CRT*) by the current of scattered electrons that impinges on the annular detector (*det*).

an image on a cathode-ray tube. This arrangement is possible only in a scanning transmission electron microscope, in which a very finely focused electron beam is swept, as in television, in a raster pattern over the specimen.

A second difficulty stems from the relatively small proportion of electrons scattered by the light atoms of biological matter. The resulting small scatter signal makes adjustment and focusing of the conventional fixed-beam electron microscope a virtual impossibility. The signal must be increased in two ways: first, by increasing the illumination with the use of inordinately large condenser apertures in the microscope, and second, by more efficient collection of the scattered electrons with as large an objective aperture as the resolving power of the microscope permits (*12*).

A third impediment is the fact that, as already mentioned, a large proportion of electrons lose energy on being scattered. These electrons cannot all be focused in the same focal plane by the magnetic field of the objective lens, as a result of a lens imperfection called chromatic aberration in analogy with light optical lenses. A sharp image results from electrons that have not suffered an energy loss, while all other electrons produce superposed images, which are more and more blurred the greater the energy loss. The thicker the specimen, the greater is the proportion of electrons scattered with a change in energy, and the greater the blurring of the image. With energy filtration, as described below, the sharp image can still be extracted even from a thick specimen; but with conventional microscopes, the only recourse is to make the specimen exquisitely thin. An exception occurs in the scanning transmission electron microscope which, because it has no lenses after the electrons traverse the specimen, has no chromatic aberrations.

To visualize macromolecules, which in general are naturally rather thin specimens, it is imperative that the support films on which they are held be exceedingly thin. The reasons are easily understood. On the one hand, the ratio of molecule thickness to support film thickness should be high, since it provides the contrast in the image and therefore determines the visibility of the object. On the other hand, a thick support film would act like a thick specimen and thus not only decrease contrast, but also appear blurred in the image from chromatic aberrations, making focusing and adjustment of astigmatism of the microscope very difficult.

Macromolecules and Tissue Sections

The approaches above permit relatively aberration-free operation of the microscope, sufficient illumination to focus, and enough contrast to distinguish even unstained specimens. This is seen for the three representative macromolecules shown in Fig. 4. The micrograph (Fig. 4a) of the small portion of highly purified unstained DNA of bacteriophage λ (*13*) indicates that in a portion of the image the two-dimensional projection of the three-dimensional double helix is easily recognized. The rest of the structure appears to have been damaged to some degree, which might be expected to happen as a result of the tremendous hail of electrons impinging on the molecule as its image is being recorded (see below). Yet in spite of the potential for such damage, repeated 0.5-nm detail has been observed in molecules such as protamine (Fig. 4b) (*14*), a nuclear protein with a molecular weight of 4000. The distinct finger-like detail in Fig. 4b, seen by now in more than 250 images of the molecule, prompted the attempt at construction of a three-dimensional atomic model (Fig. 4c), using micrographs as geometric constraints for the possible tertiary folding of primary and secondary structure derived from biochemical and physicochemical data on the molecule (*15*).

Dark field micrographs of even smaller molecules such as valinomycin (molecular weight 1111) have sufficient contrast to show the overall shape of the structure, but relevant detail within such a shape is discerned above the background mottle only when many such images are averaged (Fig. 4d) (*16, 17*). In this case, one can see a small white signal inside the white ring of the peptide-like molecular chain. This can be interpreted as the image of a potassium atom, since this detail was not seen when potassium was omitted from the specimen preparation (*16*). For other molecules of similar size, micrographic evidence was obtained for the location of calcium, barium, and iodine (*16, 17*). Comparison of this image with the structure determined crystallographically for valinomycin shows re-

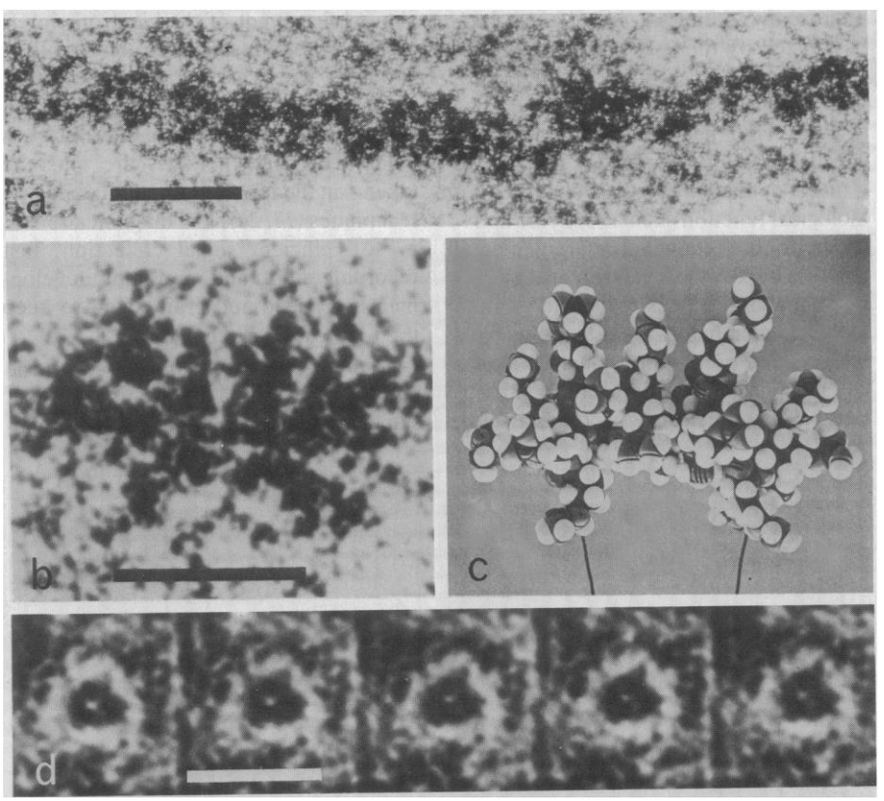

Fig. 4. (a) Dark field image of a small portion of unstained, pure double-stranded DNA of bacteriophage λ on a very thin carbon support. The left-hand portion of the image is relatively well preserved, while radiation-induced structural alterations are evident in the right half. Scale bar, 4.0 nm. (b) Dark field image of unstained purified herring protamine on carbon support. Scale bar, 2.0 nm. (c) Space-filling atomic model of protamine built from biochemical and physicochemical data, using micrographs such as (b) as a geometric constraint on the folding of the amino acid chain. (d) Optically averaged images of 20 different oriented dark field electron micrographs of the potassium complex of valinomycin. Technical details of the process are given in (*16*) and (*17*). Scale bar, 2.0 nm.

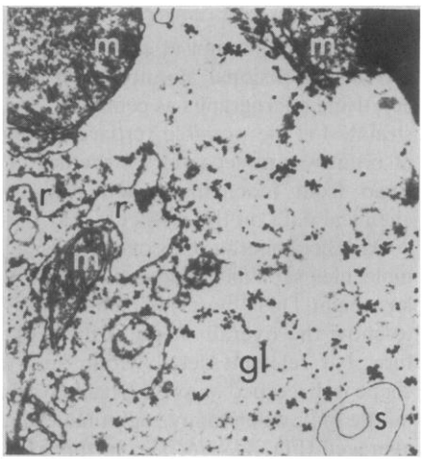

Fig. 5. Dark field micrograph of a very thin unstained section of a portion of a liver cell, fixed with glutaraldehyde and osmium. Although printed on soft photographic paper, the micrograph exhibits exceptional contrast, all expected organelles and intracellular particles being easily visible. Abbreviations: (*m*), mitochondrion; (*r*) and (*s*), rough and smooth endoplasmic reticulum; and (*gl*), glycogen.

markable agreement even for this small a molecule (*18*).

The observation of tissue sections, the most prevalent application of electron microscopy in biology, is only marginally assisted by the use of scattered electrons alone. Conventional techniques of imaging have evolved for nearly five decades, with the use of both general and specific heavy metal contrast agents. But if finer details are to be observed, if biological function such as enzyme activity is to be retained, or if elemental analysis by x-ray or electron energy loss microanalysis is desired, heavy atom stains or even heavy atom fixatives used in specimen preparation must be avoided. Then dark field microscopy, particularly of thin sections, becomes useful, since the loss in contrast due to the avoidance of stain is more than recouped by imaging with scattered electrons alone (*19*). The section of the unstained liver cell in Fig. 5 is so thin that the glycogen in the cell appears as individual granules rather than as the usual granule clusters. Nevertheless, the contrast in this dark field micrograph, made only with scattered electrons, is as high as or higher than that in conventional bright field micrographs of heavily stained specimens.

Radiation Damage and Noise

The fine detail seen in dark field images of individual macromolecules, such as that of protamine in Fig. 4b, does not come without a price. Bonds of 5 electron volts between neighboring atoms in a molecule are no match for an imaging electron with an energy of 80 or 100 kiloelectron volts. Yet, about 1500 electrons impinge on every square angstrom of specimen area in order to gather a sufficient number of scattered electrons on the photographic plate to define statistically detail as fine as 0.5 nm. Only about 1.5 percent of the electrons interact with the thin specimen, but the total exposure necessary to image molecules is nevertheless so heavy that they are invariably destroyed while their image is being recorded. In fact, care must be taken—in the form of minimum exposure techniques (*14, 20*), low magnification (*3*, p. 12), efficient signal collection, fast recording film, and optimum development for speed and grain size—to keep the total exposure this low.

Minimum exposure means that the number of electrons used to image is just sufficient to discern a particular molecule. Since this minimum number is extremely high, it becomes questionable in any individual image whether a particular fine detail is still a real representation of the original structure, is a radiation-induced structural alteration, or is merely there as a random noise fluctuation. Only repeated observation of the same detail, or enhancement of the detail in the average of many images, brings a greater certitude to its interpretation (for instance, see Fig. 4d), although verification by chemical modification on the basis of the image structure, as has been carried out for protamine, valinomycin, and vasopressin, will attest to its reality (*15–17*).

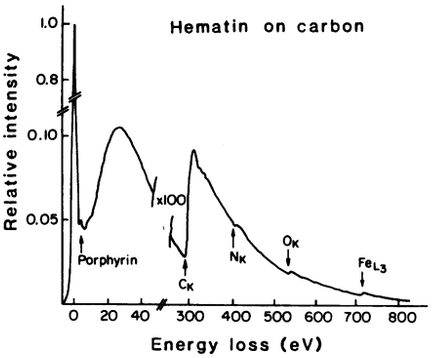

Fig. 7. Electron energy loss spectrum of 80-kilovolt electrons scattering from a thin film of hematin molecules on carbon. At 3 eV the absorption corresponding to the 400-nm light optical blue absorption of the porphyrin ring is detected, while at higher energies the *K*-electron excitations of carbon, nitrogen, and oxygen are seen, as well as the *L*-electron excitation of iron. The carbon excitation is due to both the hematin molecule and the carbon support.

Nevertheless, individual images such as Fig. 4, a and b, suggest very strongly that 0.5-nm detail is meaningful. In addition, however, direct evidence for such conclusions can be reached from the Fourier analysis of images of a periodic structure such as the alpha helix of polylysine (*21*). The rodlike superstructure of the stiff helix is just detectable directly in the dark field micrograph (Fig. 6a), becoming somewhat more easily seen when the micrograph is deliberately blurred in printing (Fig. 6b). For detail finer than this, the noise or mottle in the micrograph appears overwhelming to the eye. However, optical diffraction or digital Fourier transformation of such images clearly indicates the presence of the alpha-helical repeat distance. While the results are still preliminary, the analysis to date from 30 such rod-shaped images of polylysine shows clear maxima between 0.4 and 0.6 nm, indicating a repeat distance of 0.53 ± 0.01 nm (standard error) and a helical pitch angle of 27 ± 1.1°

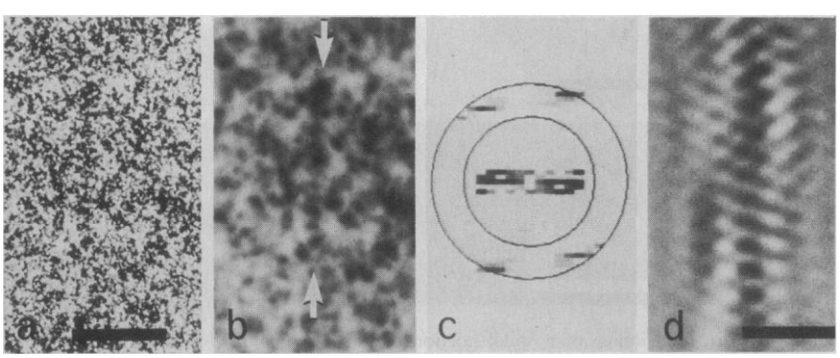

Fig. 6. A single alpha-helical molecule of polylysine on a thin carbon film. (a) Dark field electron micrograph showing a barely detectable rodlike structure. Scale bar, 5.0 nm. (b) Same image as (a) deliberately blurred to suppress fine detail and showing the rodlike structure (arrows) to advantage. (c) Computed Fourier transform of the rod in (a) showing the computer-selected strongest reflections between 0.4 and 0.6 nm delineated by the circles and low-frequency reflections around the central spot. These reflections and their immediate surroundings were used to reconstruct the image of the rodlike structure shown enlarged in (d). Scale bar, 2.0 nm.

(*22*). By comparison, the perfect alpha helix has parameters of 0.54 nm and 26°, respectively. Filtered computer reconstruction of such micrographs is not necessary for this analysis. However, reconstruction with low-frequency reflections and the four computer-selected strongest diffraction spots and their immediate surroundings between 0.4 and 0.6 nm (between the circles in Fig. 6c) is informative, since it indicates which structures give rise to the reflections. In this case, this treatment results in the rodlike structure shown enlarged in Fig. 6d. Periodicity is evident throughout the length of the rod. Moreover, in the top half and near the bottom the helical character of the molecule appears to be reflected in the zigzag structure of the reconstructed image, while below the central region, disruption of the helix is evident. Predictably, reconstruction of similar reflections from random noise patterns does not give rise to helical rod-shaped structures. Image analysis and processing thus greatly assist the elucidation of preservation or disruption of structure, here at the 0.5-nm level, that is submerged by noise in the original image.

The results above show that imaging of unstained biological specimens by scattered electrons only, although difficult because of changes in technique and in specimen preparation, brings a benefit in contrast for sectioned material, while for macromolecules it has a clear advantage in contrast, with an order of magnitude improvement in spatial resolution. Some random radiation-induced structural alterations and an unaccustomed degree of noise in the image are necessarily, although grudgingly, accepted as the cost for information that can otherwise not be obtained for single aperiodic molecules. For naturally occurring periodic structures, or such structures produced artificially, both noise and radiation damage can be reduced substantially (*6*).

Elemental Analysis

High-resolution spatial information and contrast are not the only benefits from the use of scattered electrons. A high proportion of the latter carry information about the type of atom that the electron has excited in the interaction. This chemical information has so far generally been gathered by analyzing the energy of the x-rays that are emitted by the atoms on de-excitation. The small yield of such x-rays on present-day detectors has resulted in application of this method mostly for spot analyses of local areas at low spatial resolution (~ 20 nm in diameter) (*23*). Since the yield decreases with decreasing atomic number of the element, light atoms such as oxygen, nitrogen, and carbon are virtually never analyzed.

The primary event—excitation by the imaging electron of the atom in the specimen—increases with decreasing atomic number. Therefore, as a technique complementary to x-ray microanalysis, it seems natural to analyze the spectrum of energies of the electrons after they have traversed the biological specimen. This type of analysis is carried out fairly easily by use of a sector magnet accessory (*24*). We use a more complex electron energy filter of the prism-mirror-prism (PMP) type, described originally by Castaing and Henry (*25, 26*), for such analysis as well as for imaging or elemental mapping with characteristic energy bands in the spectrum.

The spectrum of a thin film of hematin (Fig. 7) illustrates both the spectral resolution and energy range of such a device. In the low-energy loss (or excitation) range, specific excitation of the porphyrin molecule at 3 eV is seen. At higher energies, absorptions of carbon (284 eV), nitrogen (402 eV), oxygen (532 eV), and iron (721 eV) are observed as stepwise increases on a continuously decreasing background. This spectrum then identifies all the elements of hematin, except for hydrogen. Quantification of such spectra is being developed in several laboratories (*27*).

The PMP electron energy filter, in addition to analysis of elements, permits very easy imaging of the two-dimensional distribution of a particular type of atom in the specimen, with a spatial resolution of about 0.5 nm (*26, 28*). The illumination is axial, identical to normal bright field operation, but the electrons that have not interacted with the specimen are cut off by the filter. The result is a dark field–like image from electrons that have been scattered with a particu-

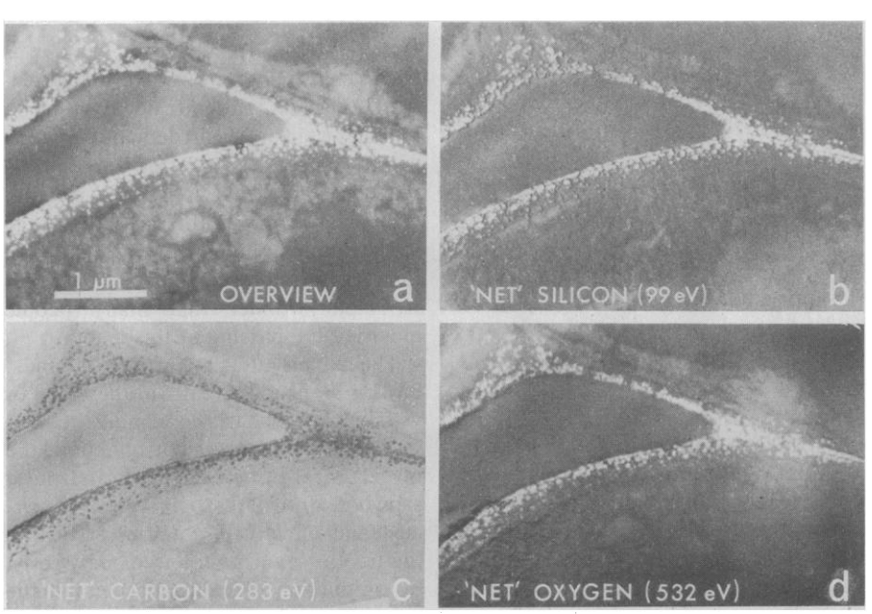

Nonselective image of the same region. Photographic processing as described in (*24*).

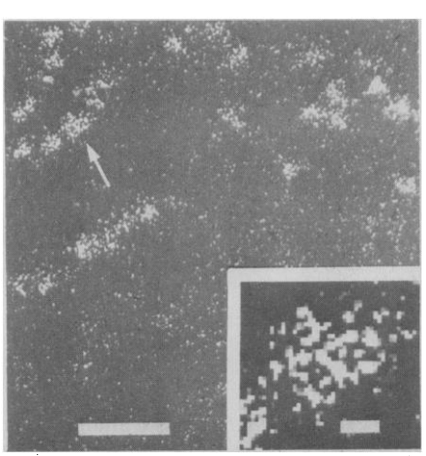

Fig. 8 (left). Elemental atomic distribution of silicon (b), carbon (c), and oxygen (d) in a section of French bean plant cells at lesion produced by the successful rejection of an incompatible rust infection. Bright areas indicate an excess of the selected element (silicon and oxygen), dark areas a deficit (carbon). (a) Fig. 9 (right). Digitally processed phosphorus elemental map of a section through part of the rough endoplasmic reticulum at the juncture of the Golgi apparatus in cells of insect fat body. Bright prominences represent the phosphorus distribution within the ribosomes. One of these (arrow) is shown enlarged in the inset. Scale bar, 100 nm; inset bar, 10 nm.

lar energy loss. Since a continuum of intensities occurs in the spectrum underneath the characteristic absorption edges (see Fig. 7), two images must be taken to obtain an elemental map: one with a narrow band of energies just above the specific absorption edge, and one just below this edge in energy. The difference between the images gives the map or spatial disrtibution of the chosen element. Figure 8 shows the net elemental distributions for silicon, oxygen, and carbon in a section of cells from a bean plant at a lesion produced by an incompatible rust infection (*21*). While silicon could be, and was, analyzed by x-ray microanalysis, the distribution of oxygen and of carbon (or the lack of the latter in this case), as well as the spatial resolution evident in the images, can only be obtained by the imaging of scattered electrons.

At higher resolutions, we have analyzed the phosphorus distributions in individual leaflets of embedded and sectioned phospholipid-containing membranes (*26, 28*), as well as the phosphorus distribution in DNA in nucleosomes (*29*). Preliminary results (Fig. 9) indicate that the distribution of phosphorus in the ribosome, delineating perhaps the ribosomal RNA, may also be amenable to study (*21*).

The good spatial resolution obtained, 0.3 to 0.5 nm (*28*); the high detection sensitivity measured, 50 atoms of 2×10^{-21} gram of phosphorus; and the short exposure time necessary, typically 5 to 15 seconds (*26*), make this technique one to two orders of magnitude better than x-ray microanalysis on each of these points. Moreover, if present applications by individual users of the device at the level of the cell membrane, the nucleosome, the Golgi apparatus, microvilli, fungal infection, bone formation, and others are an indication, the uses of energy analysis of scattered electrons in biology will be far-reaching.

References and Notes

1. F. P. Ottensmyer, E. E. Schmidt, T. Jack, J. Powell, *J. Ultrastruct. Res.* **40**, 546 (1972).
2. A. V. Crewe, J. Wall, J. Langmore, *Science* **168**, 1338 (1970); H. Hashimoto, A. Kumao, K. Hino, H. Yatsumoto, A. Ono, *Jpn. J. Appl. Phys.* **10**, 1115 (1971); R. M. Henkelman and F. P. Ottensmeyer, *Proc. Natl. Acad. Sci. U.S.A.* **68**, 3000 (1971); D. Dorignac *et al.*, *Nature (London)* **264**, 533 (1976).
3. D. J. Misell, in *Image Analysis, Enhancement and Interpretation*, vol. 7 of *Practical Methods in Electron Microscopy*, A. M. Glauert, Ed. (North-Holland, Amsterdam, 1978), p. 91.
4. A. W. Ham and D. H. Cormack, *Histology* (Lippincott, Toronto, ed. 8, 1979); C. Roland-Leeson and T. S. Leeson, *Histology* (Saunders, Philadelphia, ed. 3, 1976); K. R. Porter and M. A. Bonnevile, *An Introduction to the Fine Structure of Cells and Tissues* (Lea & Febinger, Philadelphia, 1964).
5. This apt alliterative description is due to E. Kellenberger.
6. P. N. T. Unwin and R. Henderson, *J. Mol. Biol.* **94**, 425 (1975).
7. M. H. Hahn and W. Baumeister, *Cytobiologie* **7**, 224 (1973).
8. R. D. Heidenreich, *Fundamentals of Transmission Electron Microscopy* (Interscience, New York, 1964), p. 140.
9. B. von Borris and E. Ruska, *Z. Ver. Dtsch. Ing.* **79**, 519 (1935).
10. M. von Ardenne, *Z. Tech. Phys.* **11**, 407 (1938); G. Dupouy, F. Perrier, P. Verdier, *J. Microsc. (Paris)* **5**, 655 (1966); F. P. Ottensmeyer, *Biophys. J.* **9**, 1144 (1969); J. Dubochet, in *Principles and Techniques of Electron Microscopy*, M. A. Hayat, Ed. (Van Nostrand Reinhold, New York, 1973), vol. 3, p. 113; W. Krakow, *Ultramicroscopy* **3**, 291 (1978).
11. A. V. Crewe, J. Wall, L. M. Welter, *J. Appl. Phys.* **39**, 5861 (1968).
12. F. P. Ottensmeyer, *Annu. Rev. Biophys. Bioeng.* **8**, 129 (1979).
13. I thank A. Becker for this specimen.
14. F. P. Ottensmeyer, R. F. Whiting, E. E. Schmidt, R. S. Clemens, *J. Ultrastruct. Res.* **52**, 193 (1975).
15. F. P. Ottensmeyer, R. F. Whiting, A. P. Korn, *Proc. Natl. Acad. Sci. U.S.A.* **72**, 4953 (1975).
16. F. P. Ottensmeyer, D. P. Bazett-Jones, J. Hewitt, G. B. Price, *Ultramicroscopy* **3**, 303 (1978).
17. F. P. Ottensmeyer, J. W. Andrew, D. P. Bazett-Jones, A. S. K. Chan, J. Hewitt, *J. Microsc. (Oxford)* **109**, 259 (1977).
18. M. Pinkerton, L. K. Steinrauf, P. Dawkins, *Biochem. Biophys. Res. Commun.* **35**, 512 (1969).
19. F. P. Ottensmeyer and M. Pear, *J. Ultrastruct. Res.* **51**, 253 (1975).
20. R. C. Williams and H. W. Fischer, *J. Mol. Biol.* **52**, 121 (1970).

21. I thank M. C. Heath, D. Brodie, and D. Andrews for use of their unpublished micrographs of the French bean sections, of the phosphorus map of endoplasmic recticulum, and of the polylysine helix, repectively. In addition, the use of the Dunlap Observatory flatbed microdensitometer was much appreciated.

22. D. Andrews and F. P. Ottensmeyer, *Proc. 39th Annu. Meet. Electron Microsc. Soc.* (1981), p. 34.
23. A. P. Somlyo, A. V. Somlyo, H. Shuman, M. Stewart, *Scanning Electron Microsc.* **2**, 711 (1979).
24. R. F. Egerton, *Ultramicroscopy* **3**, 39 (1978).
25. R. Castaing and L. Henry, *C. R. Acad. Sci.* **255**, 86 (1962).
26. F. P. Ottensmeyer and J. W. Andrew, *J. Ultrastruct. Res.* **72**, 336 (1980).
27. R. F. Egerton *Ultramicroscopy* **3**, 243 (1978); *ibid.* **4**, 169 (1979); D. M. Maher, in *Introduction to Analytical Electron Microscopy*, J. J. Hren, J. I. Goldstein, D. C. Joy, Eds. (Plenum, New York, 1979), p. 259; C. Colliex, C. Jeanquillaume, P. Trebbia, in *Microprobe Analysis of Biological Systems*, T. E. Hutchinson and A. P. Somlyo, Eds. (Academic Press, New York, 1981), p. 251.
28. K. M. Adamson-Sharpe and F. P. Ottensmeyer, *J. Microsc.* **122**, 309 (1981).
29. D. P. Bazett-Jones and F. P. Ottensmeyer, *Science* **211**, 169 (1981).

30. This work was supported by the Ontario Cancer Treatment and Research Foundation, the National Cancer Institute of Canada, and grant MT-3763 from the Medical Research Council of Canada.

Biological Control of Chestnut Blight

Sandra L. Anagnostakis

Chestnut blight, a classic among plant diseases, is caused by an introduced fungus that has nearly eliminated its host: the American chestnut tree (*1*). Since chestnut blight was first detected in the United States at the turn of the century, there has been no evidence of the development of genetic resistance to the disease and chemical control methods have not proved useful.

After the first infected trees were found in the Bronx Zoo in 1904 (*2*), the lethal canker organism *Endothia parasitica* (Murr.) And. spread in ever-widening circles to encompass all of the natural range of the tree. By 1950 an estimated 9 million acres (about 3.6 million hectares) of American chestnut trees were dead or dying (*3*).

American chestnut [*Castanea dentata* (Marsh) Bork.] was once the most important hardwood species in the eastern United States. Its beautiful wood was used extensively for furniture and woodwork. The tall, straight, decay-resistant timbers were in great demand for telegraph and fence poles and for railroad ties. The tanin extracted from chestnut bark and wood was the basis of a large leather tanning industry. The nuts were food for wildlife, livestock, and people. It is no wonder that many people mourned the passing of this giant.

The fungus attacks through wounds: broken branches, breaks in the bark, or woodpecker or bark borer holes. Growing out from the point of infection, the mycelium grows in the bark and outer sapwood until it has completely encircled and effectively "girdled" (Fig. 1) the tree or branch. The trees may resist by production of callus tissue, but the

The author is an Assistant Scientist in the Department of Plant Pathology and Botany at the Connecticut Agricultural Experiment Station, New Haven 06504.

0036-8075/82/0129-0466$01.00/0